

Probing the Local Bubble with Diffuse Interstellar Bands. III. The Northern hemisphere data and catalog

Amin Farhang^{1,2}, Habib G. Khosroshahi¹, Atefeh Javadi¹, Jacco Th. van Loon³

a.farhang@ipm.ir

Received _____; accepted _____

¹School of Astronomy, Institute for Research in Fundamental Sciences (IPM), P. O. Box 19395-5746, Tehran, Iran

²Department of Physics, Sharif University of Technology, P. O. Box 11365-9161, Tehran, Iran

³Astrophysics Group, Lennard-Jones Laboratories, Keele University, Staffordshire ST5 5BG, UK

ABSTRACT

We present a new high signal-to-noise (S/N) observations of the Diffuse Interstellar Bands (DIBs) in the Local Bubble and its surroundings. We observed 432 sightlines and obtain the equivalent widths of $\lambda 5780$ and $\lambda 5797$ Å DIBs up to distance of ~ 200 pc. All observations have been carried out by using Intermediate Dispersion Spectrograph (IDS) on 2.5 m Isaac Newton Telescope, during three years, to reach a minimum S/N ratio of ~ 2000 . All $\lambda 5780$ and $\lambda 5797$ absorptions are presented in this paper and the observed values of interstellar parameter; $\lambda 5780$, $\lambda 5797$, Na I D₁ and Na I D₂ including the uncertainties are tabulated.

Subject headings: stars: atmospheres, ISM: abundances – bubbles – clouds – lines and bands

1. Introduction

Sun is located within a hot bubble (known as the Local Bubble) with a low neutral gas density of $n(\text{H}) \sim 0.01 \text{ cm}^{-3}$ (Bohlin 1975; Weaver et al. 1977) and purportedly hot temperature ($T \sim 10^6 \text{ K}$, but see Welsh & Shelton (2009)), estimated based on the distribution of diffuse soft X-ray background emission (Snowden et al. 1998). According to recent observations of neutral gases (Na I), ionized atoms (Ca II) and dust grains, the Local Bubble is depleted from these common species (Vergely et al. 2001; Lallement et al. 2003; Welsh et al. 2010). Observation of nearby hot white dwarfs within the Local Bubble, failed to detect acceptable O VI absorption level (Oegerle et al. 2000). In addition, other observations of nearby white dwarfs and hot stars also failed to detect acceptable levels of highly ionized gas such as C IV and Si IV (Bertin et al. 1995; Holberg et al. 1999) within the Local Bubble.

The 3D gas maps around the Local Bubble reveal that this cavity has a chimney like structure extended to a distance of $\sim 80 \text{ pc}$ in the Galactic Plane and up to hundreds of pc into the Halo (Vergely et al. 2001; Lallement et al. 2003; Welsh et al. 2010). Also the diffuse X-ray background emissions of the Local Bubble and its neighboring cavities, have been studied to find a relation between shape of the cavities and the soft X-ray data (Puspitarini et al. 2014). While the origin of the Local Bubble is still debated, the most plausible model is that the Local Bubble has been created as a result of a number of successive supernovae in the nearby Sco–Cen association (Smith et al. 2001).

In recent years about ~ 500 narrow to broad interstellar absorption features have been observed which are known as Diffuse Interstellar Bands (DIBs) (Herbig 1995). The carrier of these heavy molecules are unknown, however, the DIB candidates could be among an infinite number of large carbon-based "organic" molecules (Sarre 2006). DIBs are used to study different condition of ISM, for instance some outstanding DIBs in the optical

waveband are empirically known to trace the neutral phase of the interstellar medium (ISM). Also DIBs are correlated well with the color excess E_{B-V} , the neutral hydrogen and the NaI column densities (Herbig 1993; Friedman et al. 2011).

DIBs react to the strength of the UV field of the local environment (Cox et al. 2006) and DIB strength varies as a function of UV radiation toward different sightlines (Vos et al. 2011). Therefore, specific groups of UV resistant molecules, such as Polycyclic Aromatic Hydrocarbons (PAHs), fullerenes and carbon chains are commonly the more acceptable candidates for DIB carriers (Herbig 1995). DIB carriers have been ubiquitously detected everywhere, for instance, DIBs have been observed in the M31 and M33 (Cordiner et al. 2008a,b), Magellanic Clouds (van Loon et al. 2013) and beyond the Milky Way in SN host galaxies (Cox & Patat 2008).

Since the temperature of the Local Bubble is purportedly high, the typical atoms and molecules could not survive in such an environments. In addition, as mentioned above, any attempts to detect other highly ionized atoms, or search for acceptable level of EUV emission have failed. Therefore we study the Local Bubble and its surroundings through DIBs in a survey over a 3 years period. We present the sightlines, spectrums, fitted profiles and the equivalent widths (EWs) for the northern hemisphere survey.

2. OBSERVATIONS

All observations have been obtained with the Intermediate Dispersion Spectrograph (IDS) at the 2.5 m Isaac Newton Telescope (INT) at the Roque de Los Muchachos in La Palma. The IDS employs a long-slit spectrograph with two CCDs: The EEV10 CCD sensitive in blue, and the RED+2 which is sensitive in the red and both CCDs have 4096×2048 pixels. The spatial scale for the EEV10 is $0''.4$ and for the RED+2 is $0''.44$

/pix, and the full unvignetted slit length is 3'.3.

For our observations we have used the 235 mm camera and H1800V IDS grating for an effective resolution of 0.31 Å/pix. H1800V was chosen since it provides a high spectral resolution well matched to the typical width of DIBs. Also we have chosen 5800 Å as the central wavelength. A 1'.1 slit yielded spectra in the 5750–6040 Å region at spectral resolutions of $R \equiv \lambda/\Delta\lambda \sim 2000$ (or a velocity resolution of $\Delta v = 150 \text{ km s}^{-1}$). The DIB detection requires a high signal-to-noise (S/N) ratio of at least 100 but for detection of very weak absorptions, as like the one was detected by Cordiner (2006) towards the nearby star $\mu^1\text{Cru}$ with $\lambda 5780$ DIB equivalent width (EW) of 4 mÅ, we need S/N of at least 2000. The seeing varied during these observing nights from 1''.1 to 1''.9.

To achieve a high quality data, we obtained more than 60 flat field frames with quartz lamp (exposure times of 13–15 sec), 15 arc frames (CuAr+CuNe) for wavelength calibration and a large number of bias frames every night. In order to achieve a minimum S/N ~ 2000 , we exposed each target 9–25 times, depending on their apparent magnitudes (see below). The data were processed using the CCDRED data reduction package and the spectrum were extracted using the KPNOSLIT package.

We have selected bright stars up to a distance of 200 pc. Targets were selected from the 3D Na I D lines survey of Welsh et al. (2010), all with well-known distances from the Hipparcos satellite (Perryman et al. 1997). Since the saturation level of the IDS detector was ~ 64000 counts, a small number of targets were rejected due to their extreme brightness ($V < 1.8 \text{ mag}$). To increase the observing run efficiency, targets with $V > 7.2 \text{ mag}$ were also rejected from our target list to avoid very long integration times. Also to maximize the uniformity of the survey, in addition to the observation of hot stars (O, B types) we also observed some cooler stars (A, F, G & K).

3. Data analysis

In DIB studies the shape of spectral profiles remain uncertain, since the carriers are unidentified. In addition, blending by that of other chemical species and possibility for blending with features from higher rotational levels of the same species (Friedman et al. 2011), make DIB studies challenging. The equivalent width is defined as:

$$W = \int \frac{I_0(\lambda) - I(\lambda)}{I_0(\lambda)} d\lambda \quad (1)$$

Where, the I_0 and I_λ are fluxes of the continuum and the spectral line respectively. With a Gaussian function one can approximate the $\lambda 5780$ and $\lambda 5797$ lines absorptions (e.g., van Loon et al. 2009). Therefore we obtain the line width in terms of the σ value of the Gaussian distribution, and then calculate the Full-Width at Half Maximum (FWHM) as $\text{FWHM} = 2(2 \ln 2)^{1/2} \sigma = 2.355\sigma$. Accordingly for producing a normalized spectrum, continuum fitting to the observed spectra was performed by fitting a nine-order Legendre polynomial.

For computing the statistical uncertainty for each observed DIB, we compute the standard deviation of residuals of the Gaussian fitting and summed in quadrature, and weighted by the Gaussian fit (van Loon et al. 2009; Vos et al. 2011). In DIB studies, the main source of error in the equivalent widths is the uncertainty in determining the real position of the continuum (systematic error), therefore the statistical error is always underestimated. For computing the systematic error, we fit three different continuum lines to local absorption region with $\pm 12 \text{ \AA}$ range around the central DIB wavelengths (linear fit to the continuum, quadratic fit to the continuum and fit to DIB with linear continuum (Kos & Zwitter 2013)). Accordingly, we set the intersection points of the DIB absorption and the continuum level (Krelowski & Sneden 1993). Therefore, the systematic uncertainty

is determined by the difference between the highest and lowest values of equivalent width among these three EWs.

For extracting the ISM absorption of cold stars, it is necessary to simulate the spectrum of cold stars. For constructing the synthetic spectrum of cold stars, we calculate the atmosphere models with the ATLAS9 code (Kurucz 1992). We use grids of ATLAS9 model atmospheres from Castelli & Kurucz (2003)¹ with the new Opacity Distribution Functions (ODFs) for several metallicities (Castelli et al. 1997). We obtained the effective temperature of the observed star and the surface gravity $\log g$ from Cayrel et al. (1996); Varenne & Monier (1999); Reddy et al. (2003); Prugniel et al. (2007); Huang et al. (2010); Prugniel et al. (2011) and Koleva & Vazdekis (2012). Also we determine target metallicity from Heacox (1979); Abt et al. (2002); Royer et al. (2002, 2007) and Schröder et al. (2009). After modeling the stellar atmosphere we generate the synthetic stellar spectrum with the Linux port of the SYNTHE suite codes (Sbordone et al. 2004; Sbordone 2005; Kurucz 2005). Atomic and molecular data were taken from the database on Kurucz website² (Kurucz 2005). Also for considering the broadening caused by rotational velocity, we use the rotational velocity from Abt et al. (2002); Royer et al. (2002, 2007) and Schröder et al. (2009). For those stars which the rotational velocity was not reported, we use $v \sin i = 15 - 20 \text{ km s}^{-1}$. In our calculations we included all the atomic and molecular lines with empirically determined atomic constants plus all the diatomic molecular lines (CH, NH, CN, MgH, SiH, SiO, H₂, C₂ and CO) except the TiO molecule.

The A-type stars have two main sources of contaminations Fe II (at 5780.13 Å and 5780.37 Å) and Fe II (at 5783.63 Å) at $\lambda 5780$ position. As well as there is no source of contamination at $\lambda 5797$. For correct these contaminations for each A-type stars that the

¹<http://wwwuser.oats.inaf.it/castelli/>

²<http://kurucz.harvard.edu>

metallicity have not been reported, we produce all possible synthetic spectra and compare them with the observed spectra. The surface gravity of A-type stars varies between 3.5 to 4.2 (Gray 1992), therefore we choose a constant $\log g = 4$ in all of our atmosphere model. From A0 to A9 spectral types, according to Theodossiou & Danezis (1991) report, we select a constant temperature for each I, II–III and IV–V luminosity classes. Also the A-type stars have different metallicities from 0 to -2 (Beers et al. 2001). Accordingly, for a given A-type subdivision (e.g., A0) and luminosity class (e.g., IV), we produce three different atmosphere models with $[\text{Fe}/\text{H}] = 0, -0.5, -1.5$, and compare with the observed spectrum to choose the best model. Also we consider the effect of rotational velocity convolved with the instrument dispersion. But the rotational velocity of our observed A-type stars are very high ($\sim 200 \text{ km s}^{-1}$) (Hoffleit & Warren 1995), thus when convolved with our instrument dispersion, the absorption lines are widened. Therefore their stellar features impact on the DIB absorption will be limited. Then we subtract the synthetic spectrum from the observed absorption (containing both stellar and interstellar absorption features). The obtained residual predominantly consists of the interstellar absorption (Montes et al. 1995a,b). Then by fitting a Gaussian function to this residual the equivalent width of the DIB will be obtain.

The spectrum shape of cool F,G, and K type stars, is similar to a two prong fork. This absorptions are caused by the presence of Fe II, Mn I, Si I (all near 5780.1 \AA) and Cr I (5781.1 \AA). Therefore for producing the synthetic spectrum of these cool stars, we consider a Gaussian profile for $\lambda 5780$ absorption lines:

$$D(\lambda) = a \exp \left(-\frac{(\lambda - b)^2}{2\sigma} \right) + c \quad (2)$$

After confirming the average $\lambda 5780$ DIB profile in an iterative procedure, according to Eq. 2, we change the a (peak intensity), b (peak center) and σ (peak with) for each

wavelength (λ) to produce a new spectrum. Then add this spectrum with the corresponding synthetic spectrum, and in each iteration according to Eq. 3, calculate the difference of the re-produced spectrum with the real observed absorption (χ^2). Eventually, the best DIB profile estimation is one with the smallest χ^2 value.

$$\chi^2 = \sum_{i=1}^N \left(\frac{(F(\lambda_i) - D(\lambda_i))^2}{F_{\text{err}}(\lambda_i)^2} \right) \quad (3)$$

We show in plot the observed spectra and their best Gaussian fit to $\lambda 5780$ and $\lambda 5797$ features. The red fits are those with acceptable DIB absorption and the blue fits are those that we are not confident about DIB character. Also the table shows the first 10 samples of $\lambda 5780$ equivalent width and its uncertainty, the $\lambda 5797$ equivalent width and its uncertainties, the Na I D₂ and Na I D₁ and their uncertainties and the target distances. Last three columns are the $\lambda 5780$, $\lambda 5797$ and Na I flags, which 1 means the quality of measurements are acceptable and 0 means unacceptable values. The full tables and plots as soon as will be released.

We wish to thank the Iranian National Observatory (INO) and School of Astronomy at IPM for facilitating and supporting this project. The observing time allocated to this project was provided by the INO. We also wish to thank the ING staff for their support. Some of the research visits related to this project have been supported by the Royal Society International Exchange Scheme. Furthermore, we thank the referee for a thorough reading of the manuscript and useful comments and suggestions.

REFERENCES

- Abt, H. A., Levato, H., & Grosso, M. 2002, *A&A*, 573, 359-365
- Beers, T. C., Rossi, S., O'Donoghue, D., et al. 2001, *MNRAS*, 320, 451-464
- Bertin, P., Vidal-Madjar, A., Lallement, R., Ferlet, R., & Lemoine, M. 1995, *A&A*, 302, 889
- Bohlin, R. 1975, *ApJ*, 200, 402-414
- Castelli, F., Gratton, R. G., & Kurucz, R. L. 1997, *A&A*, 318, 841-869
- Castelli, F., & Kurucz, R. L. 2003, *IAUS Ser. 210, Modelling of Stellar Atmospheres*, ed. N. Piskunov, W.W. Weiss (Uppsala University, Uppsala), 20
- Cayrel de Strobel, G., Soubiran, C., Friel, E. D., Ralite, N., François, P. 1996, *VizieR Online Data Catalog*, 3200, 0
- Cordiner, M. A. 2006, Ph.D. Thesis, The University of Nottingham
- Cordiner, M. A., Cox, N. L. J., Trundle, C., et al. 2008a, *A&A*, 480, 13-16
- Cordiner, M. A., Smith, K. T., Cox, N. L. J., et al. 2008b, *A&A*, 492, 5-8
- Cox, N. L. J., Cordiner, M. A., Cami, J., et al. 2006, *A&A*, 447, 991-1009
- Cox, N. L. J., & Patat, F. 2008, *A&A*, 485, 9-12
- Friedman, S. D., York, D. G., McCall, B. J., et al. 2011, *ApJ*, 727, 33
- Gray, D. F. 1992, *The Observation and Analysis of Stellar Photospheres*, Vol. 20 (Cambridge University Press: CAS)
- Hoffleit, D., & Warren, W. H. Jr. 1995, *VizieR Online Data Catalog*, 5050, 0
- Herbig, G. H. 1993, *ApJ*, 407, 142-156

Herbig, G. H. 1995, *ARA&A*, 33, 19-74

Heacox, W. D. 1979, *ApJS*, 41, 675-688

Holberg, J. B., Barstow, M. A., Bruhweiler, F. C., Hubeny, I., & Green, E. M. 1999, *ApJ*, 517, 850-858

Huang, W., Gies, D. R., & McSwain, M. V. 2010, *ApJ*, 722, 605-619

Koleva, M., & Vazdekis, A. 2012, *A&A*, 538, 143

Kos, J., & Zwitter, T. 2013, *ApJ*, 774, 72

Królowski, J., & Sneden, C. 1993, *PASP*, 105, 1141-1149

Kurucz, R. L. 1992, *RMxAA*, 23, 45

Kurucz, R. L. 2005, *MmSAI*, 8, 14

Lallement, R., Welsh, B. Y., Vergely, J. L., et al. 2003, *A&A*, 411, 447-464

Montes, D., De Casto, E., Fernandes-Figueroa, M. J., Cornide, M. 1995a, *A&AS*, 114, 187-323

Montes, D., De Casto, E., Fernandes-Figueroa, M. J., Cornide, M. 1995b, *A&AS*, 109, 135-145

Oegerle, W. R., et al. 2000, *ApJ*, 538, L23

Perryman, M. A. C., Lindegren, L., Kovalevsky, J., et al. 1997, *A&A*, 323, 49-52

Prugniel, P., Soubiran, C., Koleva, M. & Le Borgne, D. 2007, *VizieR Online Data Catalog*, 3251, 0

Prugniel, P., Vauglin, I., & Koleva, M. 2011, *A&A*, 531, A165

- Puspitarini, L., Lallement, R., Vergely, J. L., & Snowden, S. L. 2014, *A&A*, 566, AA13
- Royer, F., Grenier, S., Baylac, M. O., Gómez, A. E., & Zorec, J. 2002, *A&A*, 393, 897-911
- Reddy, B. E., Tomkin, J., Lambert, D. L., & Allende Prieto, C. 2003, *MNRAS*, 340, 304-340
- Royer, F., Zorec, J., & Gómez, A. E. 2007, *A&A*, 463, 671-682
- Sarre, P. J. 2006, *JMoSp*, 238, 1-10
- Sbordone, L., Bonifacio, P., Castelli, F., & Kurucz, R. L. 2004, *MSAIS*, 5, 93
- Sbordone, L. 2005, *MmSAI*, 8, 61
- Schröder, C., Reiners, A., & Schmitt, J. H. M. M. 2009, *A&A*, 493, 1099-1107
- Smith, L. J., & Gallagher, J. S. 2001, *MNRAS*, 326, 1027-1040
- Snowden, S. L., Egger, R., Finkbeiner, D., Freyberg, M., Plucinsky, P. 1998, *ApJ* 493, 715-729
- Theodossiou, E., & Danezis, E. 1991, *Ap&SS*, 183, 91-115
- van Loon, J. Th., Smith, K. T., McDonald, I., et al. 2009, *MNRAS*, 399, 195-208
- van Loon, J. Th., Bailey, M., Tatton, B. L., et al. 2013, *A&A*, 550, 108
- Varenne, O., Monier, R. 1999, *A&A*, 351, 247-266
- Vergely, J. L., Freire, F. R., Siebert, A., Valette, B. 2001, *A&A*, 366, 10161034
- Vos, D. A. I., Cox, N. L. J., Kaper, L., Spaans, M., & Ehrenfreund, P. 2011, *A&A*, 533, A129
- Weaver, R., McCray, R., Castor, J., Shapiro, P., Moore, R. 1977, *ApJ*, 218, 377-395

Welsh, B. Y., Shelton, R. L. 2009, Ap&SS, 323, 1-16

Welsh, B. Y., Lallement, R., Vergely, J. L., Raimond, S. 2010, A&A, 510, A54

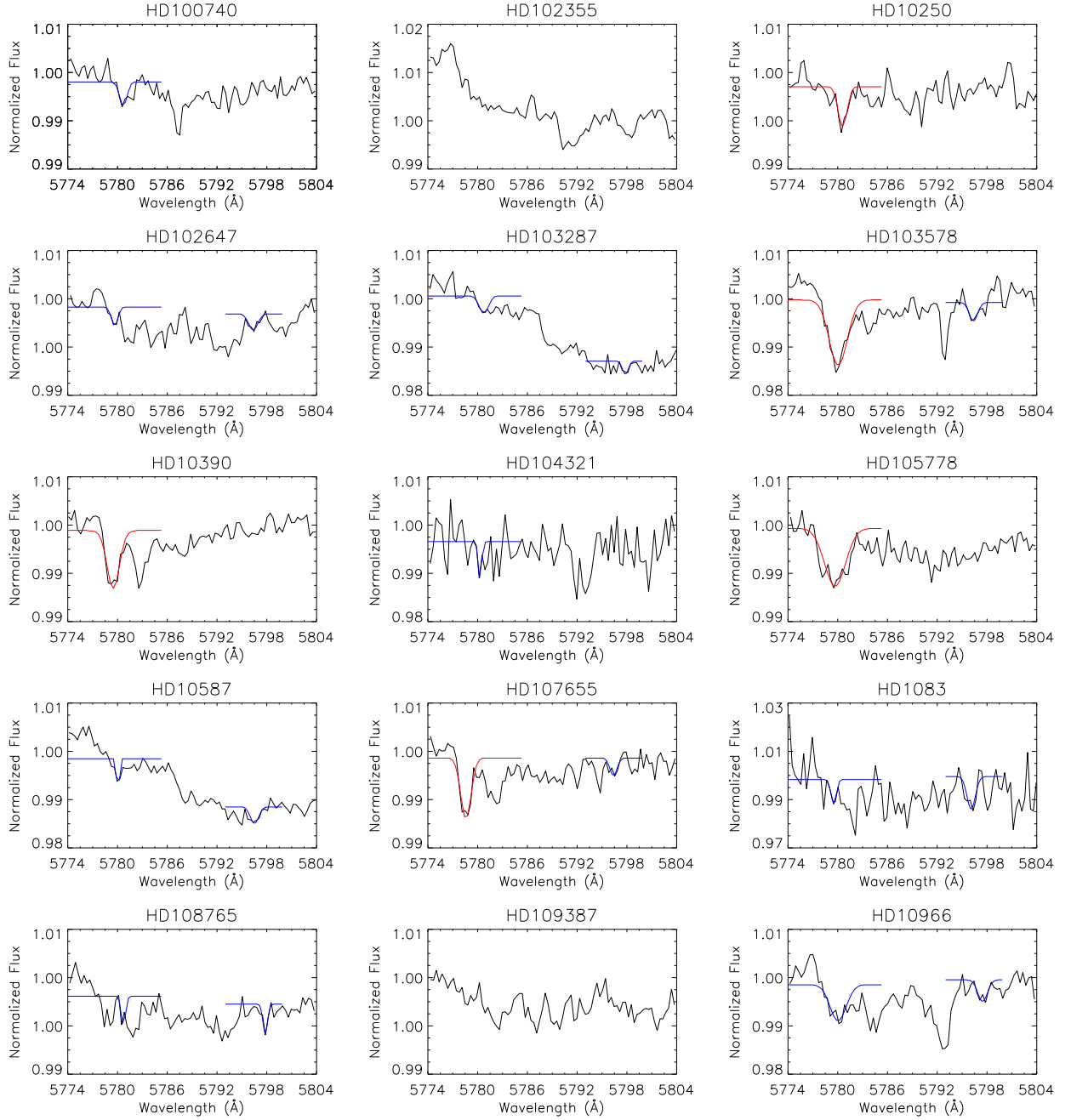


Fig. 1.— The observed spectrum of nearby stars up to distance of ~ 200 pc. The Gaussian fitted lines are divided to two different categories; the red fitted profiles shows acceptable DIBs and the blue lines represents the uncertain DIB features.

Table 1. The EW measurments of $\lambda 5780$, $\lambda 5797$ and Na I absorptions in the northern hemisphere up to distance of ~ 200 pc.

Name	glon	glat	dis	$\lambda 5780$	err $\lambda 5780$	$\lambda 5797$	err $\lambda 5797$	Na I D ₂	err Na I D ₂	Na I D ₁	err Na I D ₁	f1	f2	f3
HD10250	127.2	8.2	86	7.47	1.95	0.00	0.00	0.00	0.00	0.00	0.00	1	0	0
HD10390	134.5	-26.5	79	16.30	2.97	0.00	0.00	0.00	0.00	0.00	0.00	1	0	0
HD10587	130.2	-5.0	172	3.33	0.93	4.64	1.25	0.00	0.00	0.00	0.00	0	0	0
HD1083	113.1	-34.9	126	7.75	2.74	16.42	3.14	0.00	0.00	0.00	0.00	0	0	0
HD11291	132.6	-10.9	151	0.00	0.00	0.00	0.00	46.34	12.36	69.17	11.85	1	1	1
HD11335	132.6	-10.2	152	3.53	2.10	0.00	0.00	65.42	11.72	56.51	10.97	0	0	1
HD11415	129.8	1.6	136	22.59	3.58	1.63	0.67	55.26	9.18	33.96	8.52	1	0	1
HD11946	130.2	2.7	79	6.46	1.70	0.00	0.00	0.00	0.00	0.00	0.00	1	1	0
HD12216	128.4	10.3	50	16.73	2.81	2.17	0.76	161.15	16.00	251.97	16.19	1	0	0
HD1280	115.6	-23.7	78	27.03	4.63	6.95	1.15	224.64	18.10	275.48	18.60	1	1	0

Notes Column 1: Star name (the Henry-Draper (HD) number), Column 2: galactic longitude (degree), Column 3: galactic latitude (degree), Column 4: distance (pc), Column 5: $\lambda 5780$ EW (mÅ), Column 6: $\lambda 5780$ EW uncertainty (mÅ), Column 7: $\lambda 5797$ EW (mÅ), Column 8: $\lambda 5797$ EW uncertainty (mÅ), Column 9: Na I D₂ EW (mÅ), Column 10: Na I D₂ EW uncertainty (mÅ), Column 11: Na I D₁ EW (mÅ), Column 12: Na I D₁ EW uncertainty (mÅ), Column 13: $\lambda 5780$ quality flag; 1 = acceptable and 0 = unacceptable value, Column 14: $\lambda 5797$ quality flag; 1 = acceptable and 0 = unacceptable value, Column 15: Na I quality flag; 1 = acceptable and 0 = unacceptable value.